

*Increased shear in the North Atlantic
upper-level jet stream over the past four
decades*

Article

Accepted Version

Lee, S. H., Williams, P. D. and Frame, T. H. A. (2019)
Increased shear in the North Atlantic upper-level jet stream
over the past four decades. *Nature*, 572. pp. 639-642. ISSN
0028-0836 doi: <https://doi.org/10.1038/s41586-019-1465-z>
Available at <http://centaur.reading.ac.uk/85485/>

It is advisable to refer to the publisher's version if you intend to cite from the work. See [Guidance on citing](#).

To link to this article DOI: <http://dx.doi.org/10.1038/s41586-019-1465-z>

Publisher: Nature Publishing Group

All outputs in CentAUR are protected by Intellectual Property Rights law, including copyright law. Copyright and IPR is retained by the creators or other copyright holders. Terms and conditions for use of this material are defined in the [End User Agreement](#).

www.reading.ac.uk/centaur

CentAUR

Central Archive at the University of Reading

Reading's research outputs online

1 Increased shear in the North Atlantic upper-level jet stream over the past four
2 decades

3 Simon H. Lee, Paul D. Williams, and Thomas H. A. Frame

4 *Department of Meteorology, University of Reading, Reading, U.K.*

5 **Earth's equator-to-pole temperature gradient drives westerly mid-latitude jet streams**
6 **through thermal wind balance¹. In the upper atmosphere, anthropogenic climate**
7 **change is strengthening this meridional temperature gradient by cooling the polar lower**
8 **stratosphere^{2,3} and warming the tropical upper troposphere⁴⁻⁶, acting to strengthen the**
9 **upper-level jet stream⁷. In contrast, in the lower atmosphere, Arctic amplification of**
10 **global warming is weakening the meridional temperature gradient⁸⁻¹⁰, acting to weaken**
11 **the upper-level jet stream. Therefore, trends in the speed of the upper-level jet stream¹¹⁻**
12 **¹³ represent a closely balanced tug-of-war between two competing effects at different**
13 **altitudes¹⁴. It is possible to isolate one of the competing effects by analysing the vertical**
14 **shear instead of the speed, but this approach has not previously been taken. Here we**
15 **show that, while the zonal wind speed in the North Atlantic polar jet stream at 250 hPa**
16 **has not significantly changed since the start of the observational satellite era in 1979, the**
17 **vertical shear has increased by 15% (with a range of 11–17%) according to three**
18 **different reanalysis datasets¹⁵⁻¹⁷. We further show that this trend is attributable to the**
19 **thermal wind response to the enhanced upper-level meridional temperature gradient.**
20 **Our results indicate that climate change is having a larger impact on the North Atlantic**
21 **jet stream than previously thought. The increased vertical shear is consistent with the**
22 **intensification of shear-driven clear-air turbulence expected from climate change¹⁸⁻²⁰,**
23 **which will affect aviation in the busy transatlantic flight corridor. We conclude that the**
24 **impacts of climate change and variability on the upper-level jet stream are being partly**
25 **obscured by the traditional focus on speed rather than shear.**

26 In the northern and southern hemispheres, the mid-latitude baroclinic zone of the atmosphere
27 is associated with a planetary-scale meridional temperature gradient between the equator and
28 the pole. This temperature gradient generates westerly winds that strengthen with height –
29 vertical wind shear – as a consequence of thermal wind balance¹. Using pressure as a vertical
30 coordinate, the vertical shear in the zonal wind, $-\partial u/\partial p$, is related to the meridional
31 temperature gradient, $\partial T/\partial y$, by the thermal wind balance equation:

$$-\frac{\partial u}{\partial p} = -\frac{R}{f p} \frac{\partial T}{\partial y}, \quad (1)$$

32 where R is the specific gas constant for dry air, f is the Coriolis parameter, p is pressure, and
33 y is northward distance. Aloft, the strong westerly winds generated by thermal wind balance
34 form the polar (or mid-latitude) jet stream, the speed of which is typically maximised near the
35 tropopause, where the sign of the meridional temperature gradient (and thus the sign of the
36 vertical shear) reverses. The polar jet stream is often described as eddy-driven, because
37 eddies are required to support non-zero surface westerlies. It is distinct from the subtropical
38 jet stream, which is primarily caused by poleward transport of angular momentum in the
39 Hadley cell²¹. The polar jet stream influences mid-latitude weather systems, with the storm
40 tracks being essentially a surface expression of the jet stream²². It also plays an important role
41 in commercial aircraft operations, partly because it creates strong headwinds and tailwinds on
42 busy mid-latitude flight routes²³, but also because clear-air turbulence is generated by the
43 associated intense vertical wind shear.

44 The mid-latitude meridional temperature gradients are being modified by anthropogenic
45 climate change²⁴, and the jet streams are expected to adjust in response^{23–25}. In the lower
46 troposphere of the northern hemisphere, Arctic amplification caused primarily by lapse-rate
47 feedbacks²⁶ is weakening the meridional temperature gradient and polar jet stream^{8–10}. In
48 contrast, in the upper troposphere and lower stratosphere, the meridional temperature gradient

49 is strengthening because of the combined effects of polar lower-stratospheric cooling and
50 tropical upper-tropospheric warming, the latter caused by water vapour feedbacks releasing
51 additional latent heat and reducing the lapse rate⁷. The vertically integrated thermal wind
52 response is a tug-of-war between these two competing effects, with Arctic amplification
53 acting to decrease the wind speed in the upper troposphere and lower stratosphere, but polar
54 lower-stratospheric cooling and tropical upper-tropospheric warming acting to increase it.
55 These competing influences suggest that upper-level trends in the jet stream may be better
56 discerned through changes in vertical wind shear rather than absolute wind speed.

57 Here we analyse historic trends in the upper-level vertical wind shear over the North Atlantic.
58 In future climate projections, the prevalence of clear-air turbulence at typical aircraft cruising
59 altitudes increases more here than anywhere else globally²⁰. We use data from the ERA-
60 Interim reanalysis at 0.75° horizontal resolution¹⁶, the NCEP/NCAR reanalysis at 2.5°
61 horizontal resolution¹⁵, and the JRA-55 reanalysis at 1.25° horizontal resolution¹⁷. The use of
62 three independently produced reanalysis datasets allows us to quantify the sensitivity of our
63 results to uncertainties in the state of the atmosphere. We take six-hourly data from the years
64 1979–2017 inclusive. We restrict the temporal coverage to the satellite era, because the
65 sparsity of upper-level wind observations over the North Atlantic before 1979 substantially
66 increases uncertainty in reanalysis datasets²⁷. We consider data within the region defined by
67 30–70°N and 10–80°W. This latitudinal range is chosen to include the polar jet stream (and
68 the busy transatlantic flight corridor) whilst excluding the subtropical jet stream. We focus on
69 the shear at a pressure altitude of 250 hPa, corresponding to the climatological core of the
70 polar jet stream, and equating to a typical aircraft cruising altitude of around 34,000 feet.

71 We begin by analysing annual-mean upper-level temperature trends. As shown in **Figure 1**,
72 all three reanalysis datasets indicate a strengthening of the mid-latitude meridional
73 temperature gradient at 250 hPa. The 250 hPa pressure surface evidently intersects the

74 tropopause at around 50–60°N, with lower-stratospheric cooling on the poleward side and
75 upper-tropospheric warming on the equatorward side. The upper-tropospheric warming trend
76 is slightly stronger in ERA-Interim and JRA-55, and the lower-stratospheric cooling trend is
77 slightly stronger in NCEP/NCAR. Despite these minor differences, the spatial patterns and
78 magnitudes of the temperature trends are broadly consistent across the datasets. Unlike the
79 warming trends, the cooling trends are generally not statistically significant (except near
80 Iceland in NCEP/NCAR), probably because of large inter-annual variability associated with
81 the northern hemispheric circumpolar vortex²⁸.

82 To assess the vertical structure of the trends in the meridional temperature gradient, we
83 calculate a bulk north–south temperature difference across the North Atlantic using a two-box
84 method. On each pressure surface, annual-mean temperatures are averaged within a polar box
85 (50–70°N, 10–80°W) and then subtracted from those averaged within a subtropical box (30–
86 50°N, 10–80°W). This calculation yields a zonal-mean bulk meridional temperature
87 difference, and the trends in this quantity are shown in **Figure 2**. There is good agreement
88 between the reanalysis datasets, with all three showing a significant weakening of the
89 meridional temperature gradient in the lower atmosphere and a significant strengthening in
90 the upper atmosphere. There is a transition between these two influences at around 450 hPa.
91 There are some minor discrepancies, with NCEP/NCAR showing both a faster weakening of
92 the meridional temperature gradient in the lower atmosphere and a faster strengthening aloft.
93 At 250 hPa, however, all three reanalysis datasets show a significant strengthening of the
94 temperature difference by nearly 0.2 K decade⁻¹, consistent with **Figure 1**.

95 To assess the impacts of the increasing meridional temperature gradient at 250 hPa on the
96 atmospheric circulation, time series of the annual-mean vertical shear in zonal wind, averaged
97 over the region 30–70°N and 10–80°W, are shown in **Figure 3 (a)**. All three reanalysis
98 datasets are clearly in good agreement with respect to the inter-annual variability and the

99 superimposed upward trend. The multi-reanalysis ensemble-mean vertical wind shear shows
 100 a significant ($p = 0.03$) increase of 15% ($0.07 \text{ m s}^{-1} (100 \text{ hPa})^{-1} \text{ decade}^{-1}$) over the 39-year
 101 period. The individual increases range from 11% in JRA-55 ($0.06 \text{ m s}^{-1} (100 \text{ hPa})^{-1} \text{ decade}^{-1}$,
 102 $p = 0.09$) to 17% in ERA-Interim ($0.08 \text{ m s}^{-1} (100 \text{ hPa})^{-1} \text{ decade}^{-1}$, $p = 0.02$) and 17% in
 103 NCEP/NCAR ($0.08 \text{ m s}^{-1} (100 \text{ hPa})^{-1} \text{ decade}^{-1}$, $p = 0.01$). In contrast, as shown in **Figure 3**
 104 **(b)**, the annual-mean zonal wind speed averaged over the same region at 250 hPa has not
 105 significantly changed in any of the three datasets ($p = 0.72$ for the slope of the ensemble-
 106 mean trend). It is notable that there is less spread between the three datasets for the shear than
 107 the speed, possibly because the speed is biased low in NCEP/NCAR because of the relatively
 108 coarse resolution compared to ERA-Interim and JRA-55, whereas this bias evidently
 109 disappears when vertical differences are taken to compute the shear.

110 The increased shear without increased speed shown for the upper atmosphere in **Figure 3**
 111 indicates that the weaker meridional temperature gradient (and weaker vertical wind shear) in
 112 the lower troposphere is masking the stronger meridional temperature gradient (and stronger
 113 vertical wind shear) in the upper troposphere and lower stratosphere, through a large degree
 114 of cancellation in the vertically integrated thermal wind. We illustrate this effect by showing
 115 vertical profiles of trends in shear and speed throughout the depth of the troposphere in
 116 **Extended Data Figure 1**. The shear is strengthening within the jet core as well as throughout
 117 the broader region influenced by the jet stream (**Extended Data Figure 2**) and the trends are
 118 not attributable to a shift in the annual-mean latitude of the jet core (**Extended Data**
 119 **Figure 3**).

120 To relate trends in the meridional temperature gradient to trends in the vertical shear, we
 121 invoke the time derivative of the thermal wind balance equation (1):

$$-\frac{\partial}{\partial t} \frac{\partial u}{\partial p} = -\frac{R}{f p} \frac{\partial}{\partial t} \frac{\partial T}{\partial y}. \quad (2)$$

122 We calculate both sides of this equation independently at each grid-point, as a measure of the
123 extent to which the vertical wind shear changes are attributable to the local thermal wind
124 response to the meridional temperature gradient changes. The time derivatives are evaluated
125 as the linear trends over the period 1979–2017, calculated by applying ordinary least-squares
126 regression to annual-mean values of $\partial u/\partial p$ and $\partial T/\partial y$ at each grid-point on the 250 hPa
127 pressure surface. Maps of the left side of equation (2) – the directly calculated vertical wind
128 shear trend, produced by differencing the wind fields at the two adjacent pressure levels – are
129 shown in **Figure 4 (a, b, c)**. Maps of the right side of equation (2) – the expected vertical
130 wind shear trend, produced by using the temperature field and assuming thermal wind
131 balance – are shown in **Figure 4 (d, e, f)**. There is a clear trend towards stronger vertical
132 shear at 250 hPa over almost the entire North Atlantic domain in all three reanalysis datasets.
133 The trend is statistically significant in the core of the climatological jet stream and on the
134 poleward flank. We note the similarity in spatial patterns between these observed vertical
135 wind shear increases and future projections of increased clear-air turbulence^{18,19}. The good
136 agreement between the left and right sides of equation (2), in terms of both the spatial
137 patterns (the pattern correlation coefficients are $r > 0.70$ in all three datasets) and magnitudes,
138 confirms that the vertical wind shear trends are indeed largely attributable to the response of
139 the thermal wind to the meridional temperature gradient trends. The small discrepancies are
140 presumably attributable to the numerical finite differences used to estimate the derivatives, as
141 well as to weak ageostrophic and non-hydrostatic effects.

142 In summary, we have identified the first observationally based evidence of increased vertical
143 wind shear in the North Atlantic upper-level jet stream over the satellite era (1979–2017).
144 The increase of 15% (with a range of 11–17%) is statistically significant, is present in three
145 independently produced reanalysis datasets, and is attributable to the thermal wind response
146 to the strengthening upper-level meridional temperature gradient. The stronger shear is

147 consistent with the intensification of clear-air turbulence expected from climate change¹⁸⁻²⁰,
148 because clear-air turbulence is generated by strong vertical wind shear (which means small
149 Richardson number; we note that a 15% shear increase implies roughly a 30% Richardson
150 number decrease, because of their inverse square relationship). In contrast to the large
151 increase in vertical wind shear, we find that the zonal wind speed has not significantly
152 changed, consistent with previous studies^{11,12}. The explanation for this effect is that, in the
153 vertically integrated thermal wind balance equation, the weaker meridional temperature
154 gradient and weaker vertical wind shear in the lower troposphere are mostly offsetting the
155 stronger meridional temperature gradient and stronger vertical wind shear aloft. Increased
156 vertical wind shear has important implications, not only for clear-air turbulence and its
157 impacts on aviation, but also for the turbulent mixing of atmospheric constituents across the
158 tropopause²⁹, with potentially significant consequences for large-scale atmospheric
159 thermodynamics and dynamics³⁰.

160 Our results indicate that climate change is having a larger impact on the North Atlantic jet
161 stream than previously thought. We conclude that the impacts of climate change and
162 variability on the upper-level jet stream are being partly obscured by the traditional focus on
163 speed rather than shear. We suggest that climate-modelling studies into the response of the jet
164 streams to climate change should therefore include consideration of the vertical shear as well
165 as the speed. We anticipate that inter-model differences in upper-level vertical wind shear
166 trends will have a clear interpretation in terms of different upper-level temperature trends. On
167 the other hand, inter-model differences in upper-level wind speed trends may be more
168 difficult to interpret, because of different balances in the competition between temperature
169 trends at upper and lower levels.

170 **References**

- 171 1. Wallace, J. M. & Hobbs, P. V. *Atmospheric Science: An Introductory Survey*.
172 (Academic Press, 2006).
- 173 2. Held, I. M. Large-Scale Dynamics and Global Warming. *Bull. Am. Meteorol. Soc.* **74**,
174 228–241 (1993).
- 175 3. Thompson, D. W. J. & Solomon, S. Recent stratospheric climate trends as evidenced
176 in radiosonde data: Global structure and tropospheric linkages. *J. Clim.* **18**, 4785–4795
177 (2005).
- 178 4. Allen, R. J. & Sherwood, S. C. Warming maximum in the tropical upper troposphere
179 deduced from thermal winds. *Nat. Geosci.* **1**, 399–403 (2008).
- 180 5. Mitchell, D. M., Thorne, P. W., Stott, P. A. & Gray, L. J. Revisiting the controversial
181 issue of tropical tropospheric temperature trends. *Geophys. Res. Lett.* **40**, 2801–2806
182 (2013).
- 183 6. Sherwood, S. C. & Nishant, N. Atmospheric changes through 2012 as shown by
184 iteratively homogenized radiosonde temperature and wind data (IUKv2). *Environ. Res.*
185 *Lett.* **10**, 054007 (2015).
- 186 7. Lorenz, D. J. & DeWeaver, E. T. Tropopause height and zonal wind response to global
187 warming in the IPCC scenario integrations. *J. Geophys. Res. Atmos.* **112**, 1–11 (2007).
- 188 8. Francis, J. A. & Vavrus, S. J. Evidence linking Arctic amplification to extreme
189 weather in mid-latitudes. *Geophys. Res. Lett.* **39**, 1–6 (2012).
- 190 9. Haarsma, R. J., Selten, F. & van Oldenborgh, G. J. Anthropogenic changes of the
191 thermal and zonal flow structure over Western Europe and Eastern North Atlantic in
192 CMIP3 and CMIP5 models. *Clim. Dyn.* **41**, 2577–2588 (2013).
- 193 10. Francis, J. A. & Vavrus, S. J. Evidence for a wavier jet stream in response to rapid

- 194 Arctic warming. *Environ. Res. Lett.* **10**, 014005 (2015).
- 195 11. Archer, C. L. & Caldeira, K. Historical trends in the jet streams. *Geophys. Res. Lett.*
196 **35**, 1–6 (2008).
- 197 12. Pena-Ortiz, C., Gallego, D., Ribera, P., Ordonez, P. & Del Carmen Alvarez-Castro, M.
198 Observed trends in the global jet stream characteristics during the second half of the
199 20th century. *J. Geophys. Res. Atmos.* **118**, 2702–2713 (2013).
- 200 13. Manney, G. L. & Hegglin, M. I. Seasonal and Regional Variations of Long-Term
201 Changes in Upper-Tropospheric Jets from Reanalyses. *J. Clim.* **31**, 423–448 (2018).
- 202 14. Francis, J. A. Why are Arctic linkages to extreme weather still up in the air? *Bull. Am.*
203 *Meteorol. Soc.* **98**, 2551–2558 (2017).
- 204 15. Kalnay, E. *et al.* The NCEP/NCAR 40-year reanalysis project. *Bull. Am. Meteorol.*
205 *Soc.* **77**, 437–471 (1996).
- 206 16. Dee, D. P. *et al.* The ERA-Interim reanalysis: Configuration and performance of the
207 data assimilation system. *Q. J. R. Meteorol. Soc.* **137**, 553–597 (2011).
- 208 17. Kobayashi, S. *et al.* The JRA-55 Reanalysis: General Specifications and Basic
209 Characteristics. *J. Meteorol. Soc. Japan. Ser. II* **93**, 5–48 (2015).
- 210 18. Williams, P. D. & Joshi, M. M. Intensification of winter transatlantic aviation
211 turbulence in response to climate change. *Nat. Clim. Chang.* **3**, 644–648 (2013).
- 212 19. Williams, P. D. Increased light, moderate, and severe clear-air turbulence in response
213 to climate change. *Adv. Atmos. Sci.* **34**, 576–586 (2017).
- 214 20. Storer, L. N., Williams, P. D. & Joshi, M. M. Global Response of Clear-Air
215 Turbulence to Climate Change. *Geophys. Res. Lett.* **44**, 9976–9984 (2017).

- 216 21. Lee, S. & Kim, H. The Dynamical Relationship between Subtropical and Eddy-Driven
217 Jets. *J. Atmos. Sci.* **60**, 1490–1503 (2003).
- 218 22. Hannachi, A., Woollings, T. & Fraedrich, K. The North Atlantic jet stream: A look at
219 preferred positions, paths and transitions. *Q. J. R. Meteorol. Soc.* **138**, 862–877 (2012).
- 220 23. Williams, P. D. Transatlantic flight times and climate change. *Environ. Res. Lett.* **11**,
221 024008 (2016).
- 222 24. Vallis, G. K., Zurita-Gotor, P., Cairns, C. & Kidston, J. Response of the large-scale
223 structure of the atmosphere to global warming. *Q. J. R. Meteorol. Soc.* **141**, 1479–1501
224 (2015).
- 225 25. Woollings, T. & Blackburn, M. The North Atlantic jet stream under climate change
226 and its relation to the NAO and EA patterns. *J. Clim.* **25**, 886–902 (2012).
- 227 26. Stuecker, M. F., Bitz, C. M., Armour, K. C., Proistosescu, C. & Kang, S. M. Polar
228 amplification dominated by local forcing and feedbacks. *Nat. Clim. Chang.* **8**, 1076–
229 1081 (2018).
- 230 27. Fujiwara, M. *et al.* Introduction to the SPARC Reanalysis Intercomparison Project (S-
231 RIP) and overview of the reanalysis systems. *Atmos. Chem. Phys.* **17**, 1417–1452
232 (2017).
- 233 28. Waugh, D. W., Sobel, A. H. & Polvani, L. M. What is the polar vortex and how does it
234 influence weather? *Bull. Am. Meteorol. Soc.* **98**, 37–44 (2017).
- 235 29. Shapiro, M. A. Turbulent Mixing within Tropopause Folds as a Mechanism for the
236 Exchange of Chemical Constituents between the Stratosphere and Troposphere. *J.*
237 *Atmos. Sci.* **37**, 994–1004 (1980).
- 238 30. Maycock, A. C., Joshi, M. M., Shine, K. P. & Scaife, A. A. The circulation response to

239 idealized changes in stratospheric water vapor. *J. Clim.* **26**, 545–561 (2013).

240 **Acknowledgements**

241 S.H.L. acknowledges support through a Ph.D. studentship from the Natural Environment
242 Research Council SCENARIO Doctoral Training Partnership (reference NE/L002566/1).

243 **Author contributions**

244 S.H.L. and P.D.W. jointly conceived the study. S.H.L. performed the data analysis and
245 produced the figures with input from P.D.W and T.H.A.F. All authors contributed to writing
246 the manuscript. The authors discussed the results with each other at all stages.

247 **Author information**

248 The authors declare no competing financial interests. Correspondence and requests for
249 materials should be addressed to P.D.W. (p.d.williams@reading.ac.uk).

250 **Figure 1: Annual-mean temperature trends in the North Atlantic at 250 hPa over the**
251 **period 1979–2017.** Linear trends are calculated using ordinary least-squares regression from
252 the (a) ERA-Interim, (b) NCEP/NCAR, and (c) JRA-55 reanalysis datasets. Significant
253 ($p < 0.05$; $n = 39$) trends are indicated by stippling.

254 **Figure 2: Vertical profiles of trends in the annual-mean north–south temperature**
255 **difference across the North Atlantic over the period 1979–2017.** Linear trends are
256 calculated from the (a) ERA-Interim, (b) NCEP/NCAR, and (c) JRA-55 reanalysis datasets.
257 Red and blue shading represents positive and negative trends, respectively. Error bars
258 represent the 95% confidence intervals in the slope of the ordinary least-squares regression
259 ($n = 39$).

260 **Figure 3: Time series of annual-mean wind characteristics in the North Atlantic at**
261 **250 hPa over the period 1979–2017.** Panel (a) shows the vertical shear in the zonal wind,

262 and panel (b) shows the zonal wind speed. Data are presented from the ERA-Interim,
263 NCEP/NCAR, and JRA-55 reanalysis datasets. Also shown are the mean of the three
264 reanalysis datasets and the linear trend in the mean.

265 **Figure 4: Annual-mean trends in vertical shear in zonal wind in the North Atlantic at**
266 **250 hPa over the period 1979–2017.** Panels (a), (b), and (c) show the actual vertical wind
267 shear trends calculated from the wind field, whereas panels (d), (e), and (f) show the expected
268 vertical wind shear trends calculated from the temperature field using thermal wind balance.
269 Linear trends are calculated using ordinary least-squares regression from the (a, d) ERA-
270 Interim, (b, e) NCEP/NCAR, and (c, f) JRA-55 reanalysis datasets. Significant ($p < 0.05$;
271 $n = 39$) trends are indicated by stippling. To indicate the climatological jet stream position,
272 the 1979–2017 annual-mean zonal wind at 250 hPa in each reanalysis dataset is also shown
273 (black contours every 5 m s^{-1}).

274 **Methods**

275 The North Atlantic region was chosen partly because it is the world’s busiest oceanic flight
276 corridor. Due to the zonally extended nature of the polar jet stream in this region,
277 transatlantic flights are typically affected by the strength and position of the jet stream
278 throughout their entire flight paths. The effects of the jet stream on aircraft include
279 headwinds, tailwinds, and clear-air turbulence. A further reason for choosing the North
280 Atlantic is that – unlike the North Pacific – it exhibits separate polar and subtropical jet
281 streams, allowing an analysis of the polar jet stream exclusively.

282 We used pressure-level zonal wind and temperature data from the ERA-Interim,
283 NCEP/NCAR, and JRA-55 reanalysis datasets at six-hourly analysis intervals from 1 January
284 1979 to 31 December 2017 inclusive, giving 39 full years of data. All datasets were used on a
285 standard latitude–longitude grid (0.75° for ERA-Interim, 2.5° for NCEP/NCAR, and 1.25°

286 for JRA-55). Trends were calculated using ordinary least-squares regression, and statistical
287 significance was assessed at the 95% confidence level ($p < 0.05$) according to a two-tailed t -
288 test. The effect of temporal autocorrelation on statistical significance was tested in the
289 computed annual-mean data and found to be negligible. Percentage changes were calculated
290 using the values of the fitted linear trend lines in 1979 and 2017.

291 To calculate the two-box zonal-mean bulk meridional temperature difference, we first
292 averaged the annual-mean temperature in a subtropical box (30–50°N, 10–80°W) and a polar
293 box (50–70°N, 10–80°W), with a cosine(latitude) weighting factor to account for the
294 convergence of grid points at high latitudes. The latitudinal bounds of these boxes were
295 chosen to be approximately either side of the climatological annual-mean jet stream latitude
296 in the North Atlantic. We then found the meridional temperature difference across the North
297 Atlantic by subtracting the subtropical box temperature from the polar box temperature.

298 The jet stream was analysed in the North Atlantic region (10–80°W, 30–70°N). The annual-
299 mean regional-mean 250 hPa vertical shear in zonal wind was calculated by taking a centred
300 vertical finite difference using the annual-mean zonal winds at 300 and 200 hPa:

$$-\left. \frac{\partial u}{\partial p} \right|_{250 \text{ hPa}} \approx \frac{u(200 \text{ hPa}) - u(300 \text{ hPa})}{100 \text{ hPa}}. \quad (3)$$

301 We also calculated trends in the annual-mean regional-mean (area-weighted) zonal wind
302 speed at 250 hPa over the North Atlantic region. Vertical profiles of vertical shear trends
303 were calculated by taking centred finite differences at 50 hPa intervals for ERA-Interim and
304 JRA-55, and from neighbouring pressure levels in NCEP/NCAR (due to the spacing of
305 available pressure-level data).

306 The annual-mean regional-maximum vertical shear was calculated by a similar centred-
307 difference method: we first subtracted the 300 hPa zonal wind from the 200 hPa zonal wind
308 and then found the maximum value within the North Atlantic region at each six-hourly
309 interval, before averaging the maximum values annually. For the annual-mean regional-
310 maximum zonal wind speed, we found the maximum 250 hPa zonal wind speed within the
311 North Atlantic region at each six-hourly interval, before averaging annually. In both cases,
312 the latitude at which the maximum occurred was stored.

313 When the calculations in **Figure 3** are repeated using the annual-mean regional-maximum
314 vertical shear, instead of the annual-mean regional-mean vertical shear, a significant
315 ensemble-mean increase of 11% ($p < 0.01$) in the shear is found. The individual increases are
316 10% in ERA-Interim ($p < 0.01$), 18% in NCEP/NCAR ($p < 0.01$), and 7% in JRA-55
317 ($p < 0.01$) (**Extended Data Figure 2**). These results confirm that the shear is strengthening
318 within the jet core as well as throughout the broader region influenced by the jet stream. The
319 trends are not attributable to a shift in the annual-mean latitude of the jet core, which shows
320 no significant trend over the period (**Extended Data Figure 3**).

321 We used the time derivative of the thermal wind balance equation to relate linear trends in the
322 meridional temperature gradient to linear trends in the vertical wind shear. At 250 hPa, we
323 calculated trends in the annual-mean values of $\partial u / \partial p$ (using the centred finite difference
324 method outlined above) and $\partial T / \partial y$. The agreement between the two was assessed through
325 Pearson's correlation coefficient using an area-weighted pattern correlation.

326 According to thermal wind balance, the trend in the zonal wind speed in the upper
327 troposphere and lower stratosphere is given by the vertical integral of equation (2). This
328 vertical integral is performed throughout the depth of the free troposphere, starting from the
329 top of the planetary boundary layer. Temperature gradients in the lower troposphere are

330 included in the integral, and therefore Arctic amplification at low levels is able to influence
331 the wind speed at upper levels. For example, written in equation form, we have:

$$\frac{\partial u(250 \text{ hPa})}{\partial t} = \int_{p_0}^{450 \text{ hPa}} \frac{R}{fp} \frac{\partial}{\partial t} \left(\frac{\partial T}{\partial y} \right) dp + \int_{450 \text{ hPa}}^{250 \text{ hPa}} \frac{R}{fp} \frac{\partial}{\partial t} \left(\frac{\partial T}{\partial y} \right) dp \approx 0, \quad (4)$$

332 where p_0 is the pressure at the top of the planetary boundary layer. Here, the free troposphere
333 has been divided into two layers at 450 hPa, by reference to **Figure 2**. The lower boundary
334 term $\partial u(p_0)/\partial t$ arising from the vertical integration has been neglected in equation (4),
335 because the trend in zonal wind speed in the lower troposphere is not significantly different
336 from zero in any of the reanalysis datasets, as shown in **Extended Data Figure 1 (d, e, f)**.
337 Our study shows that, on the right-hand side of equation (4), the first integral (which includes
338 the weakening low-level temperature gradient from Arctic amplification) and the second
339 integral (which includes the strengthening upper-level temperature gradient) are essentially
340 equal and opposite when averaged over the North Atlantic region, thus largely cancelling out
341 and leaving no significant trend in the upper-level speed.

342 **Data availability statement**

343 The NCEP/NCAR reanalysis data may be obtained from the National Oceanic and
344 Atmospheric Administration (NOAA) Oceanic and Atmospheric Research (OAR) Earth
345 System Research Laboratory (ESRL) Physical Sciences Division (PSD), Boulder, Colorado,
346 USA (<https://www.esrl.noaa.gov/psd/>). The ERA-Interim and JRA-55 reanalysis data may be
347 obtained from the Research Data Archive at the National Center for Atmospheric Research
348 (NCAR), Computational and Information Systems Laboratory, Boulder, Colorado, USA
349 (<https://doi.org/10.5065/D6CR5RD9> and <https://doi.org/10.5065/D6HH6H41>, respectively).

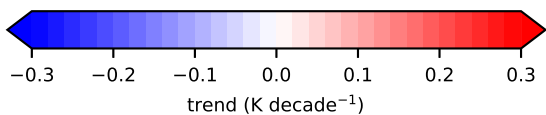
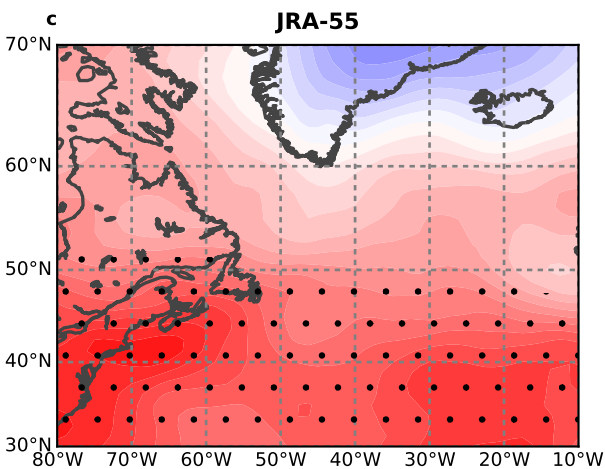
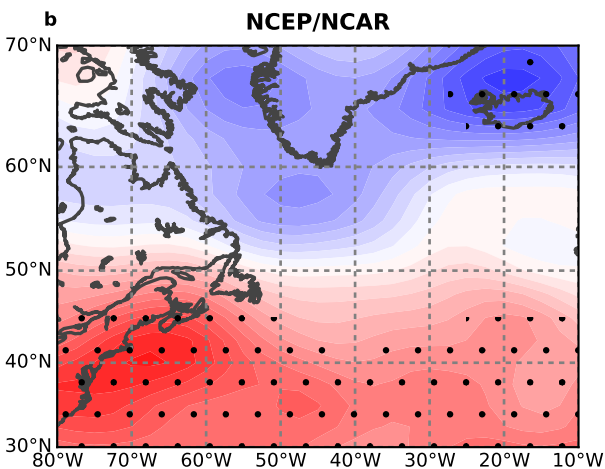
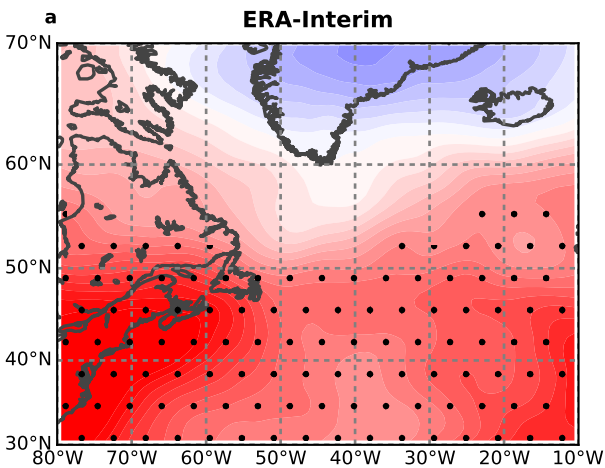
350 **Code availability statement**

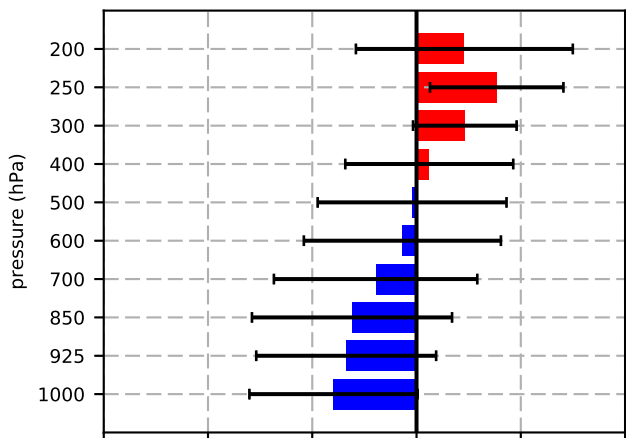
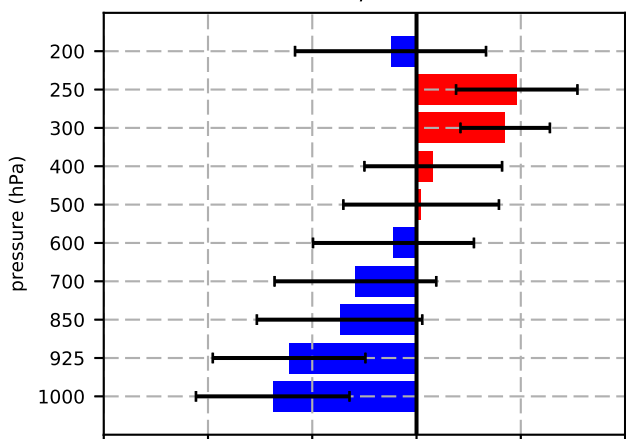
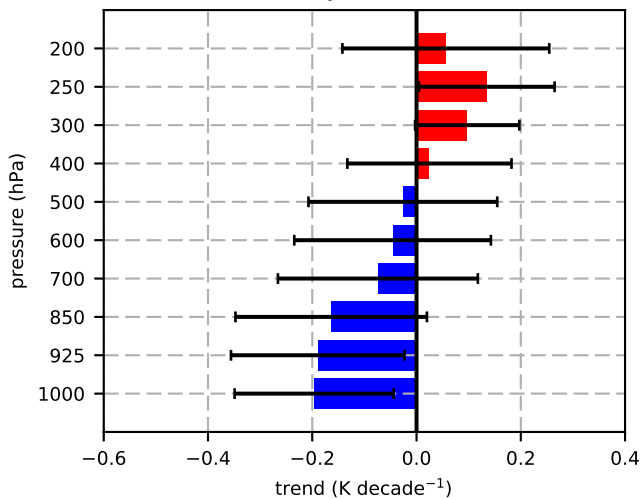
351 The analytical computer codes are publicly available at
352 <http://doi.org/10.5281/zenodo.3238842>.

353 **Extended Data Figure 1: Vertical profiles of annual-mean trends in wind characteristics**
354 **in the North Atlantic over the period 1979–2017.** Panels (a, b, c) show trends in the
355 vertical shear in the zonal wind, and panels (d, e, f) show trends in the zonal wind speed.
356 Linear trends are calculated from the (a, d) ERA-Interim, (b, e) NCEP/NCAR, and (c, f) JRA-
357 55 reanalysis datasets. Red and blue shading represents positive and negative trends,
358 respectively. Error bars represent the 95% confidence intervals in the slope of the ordinary
359 least-squares regression ($n = 39$).

360 **Extended Data Figure 2: Annual-mean regional-maximum six-hourly vertical shear in**
361 **zonal wind in the North Atlantic at 250 hPa over the period 1979–2017.** Data are
362 presented from the ERA-Interim, NCEP/NCAR, and JRA-55 reanalysis datasets. Also shown
363 are the mean of the three reanalysis datasets and the linear trend in the mean.

364 **Extended Data Figure 3: Annual-mean latitude of the core of the polar jet stream in the**
365 **North Atlantic at 250 hPa over the period 1979–2017.** Panel (a) shows the annual-mean
366 latitude of the regional-maximum six-hourly vertical shear in zonal wind, and panel (b)
367 shows the annual-mean latitude of the regional-maximum six-hourly zonal wind speed. Data
368 are presented from the ERA-Interim, NCEP/NCAR, and JRA-55 reanalysis datasets. Also
369 shown are the mean of the three reanalysis datasets and the linear trend in the mean, which
370 has a statistically insignificant slope of (a) -0.1 degrees decade⁻¹ ($p = 0.54$) and (b)
371 0.01 degrees decade⁻¹ ($p = 0.76$).



a ERA-Interim**b NCEP/NCAR****c JRA-55**

— ERA-Interim — NCEP/NCAR — JRA-55 ● mean - - - mean trend

